Wetting and Chain Packing Across Interfacial Zones Affect Distribution of Relaxations in Polymer and Polymer-grafted Nanocomposites

Emmanuel U. Mapesa,[†#] Dayton P. Street,[‡#] Maximilian F. Heres,[†] S. Michael Kilbey II,[†,‡*] and Joshua Sangoro[†*]

[†] *Department of Chemical and Biomolecular Engineering, University of Tennessee, Knoxville, Tennessee 37996*

[‡] *Department of Chemistry, University of Tennessee, Knoxville, Tennessee 37996*

For Table of Contents Use Only

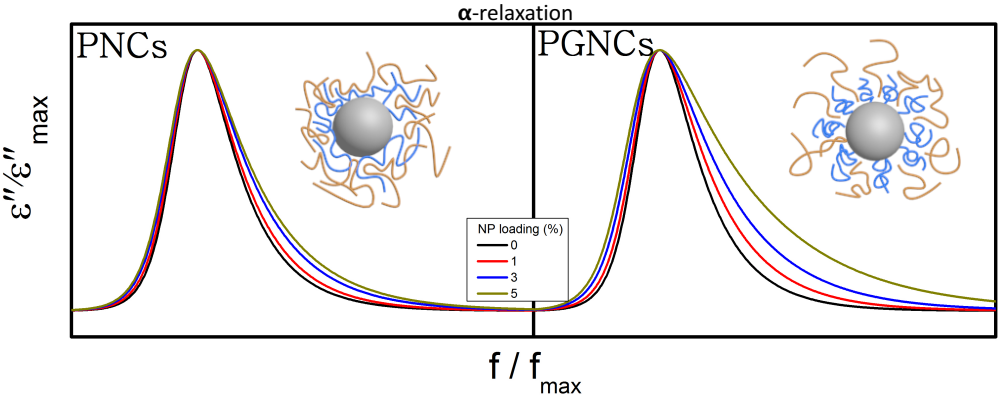

Abstract

Polymers exhibit deviations from their bulk physical properties in the vicinity of solid interfaces due to changes in configurations, entanglements, and relaxation dynamics at the interfacial regions. By comparing grafted and non-grafted polymer nanocomposite systems based on poly(methyl methacrylate) and silica, we show that the distribution of relaxation times exhibits both commonly-reported slower mobility, as well as faster modes that depend on the nature of the interfacial zone, matrix molecular weight, and loading level of nanomaterials. These findings are derived from studies using broadband dielectric spectroscopy (BDS) and differential scanning calorimetry (DSC) to probe molecular and interfacial dynamics. By systematically examining nanocomposites based on non-functionalized "bare" Si NPs dispersed in PMMA matrices and on PMMA-grafted Si NPs (PMMA-g-NPs) in PMMA matrices, we probe the effects of interfacial interactions and confinement in each of these cases on the glass transition temperature, Tg, the mean time-scales, as well as spectral shapes of the dielectric relaxation. The faster relaxation modes are attributed to the increasing importance of chain wetting and packing in the interfacial zones around nanofillers, especially in the polymer-grafted system. These insights are used to generate a unifying molecular framework that explains the enhancement in numerous macroscopic physical properties of polymer and polymer-grafted nanocomposites, which suits them for myriad applications.

Introduction

Interest in polymer nanocomposites consisting of uniformly dispersed nanoparticles (NPs) in a polymeric matrix remains high because the addition of very small amounts of nanomaterials provides a way to dramatically modify the macroscopic electrical, mechanical, or optical properties. The superposition of properties derived from hard matter and soft matter allows properties such as electrical conductivity, tensile strength, hardness, or refractive index, to be changed, suiting nanocomposites for myriad applications.[1-15] In addition to their use as structural materials, the range of potential applications for polymer nanocomposites includes electronics, optics, photovoltaics and electrochemical energy storage.

It is widely appreciated that interactions at the polymer-NP interface play a critical role in determining the macroscopic physical properties of the composite material.[11-14, 16-35] It has been demonstrated that the microscopic details of the interfacial zone – and hence the macroscopic properties of the composite – can be tuned by altering specific features of the nanoparticles, such as their shapes[30] and sizes,[27, 28, 36] the nature of the polymer-NP interactions,[33, 37] or the molecular weight[26, 28, 38] and rigidity of the matrix polymer.[29, 33] While some investigations have suggested that the chain dynamics within the interfacial layer are completely frozen,[38-41] a number of other studies have shown that the dynamics only get slower than the bulk-like segmental relaxation of the host matrix.[31-33, 42] For instance, in dielectric relaxation studies of poly(2-vinylpyridine)/silica and poly(vinyl acetate)/silica nanocomposites, Holt *et al*.[31] and Füllbrandt *et al*.[32], respectively, observe new relaxation processes. These new processes, which are slower than the primary structural relaxation of the polymer matrix, were attributed to attractive interactions between polymer chains and NP surfaces.

While most of the experimental studies that probe relaxation dynamics of polymer nanocomposites focus on systems consisting of bare nanoparticles dispersed in polymers or copolymers, there are few studies of segmental and chain relaxations in polymer nanocomposite systems having functionalized NPs.[9, 10] Nanocomposites containing polymer-grafted nanoparticles that are created *via* surface modification methods are widely used because the grafted chains mitigate the strong van der Waals interactions that drive nanoparticle aggregation. In the typical case where the graft and matrix chains are of the same chemical identity, the steric barrier conveyed by the tethered chains mediates inter-particle interactions, thereby preventing NP aggregation and promoting dispersion.[43-46] These alterations, which often are evidenced by the organization of the nanoparticles in the polymer matrix, are the result of perturbations to the range and character of interactions between the NPs and polymer matrix chains that operate at the nanoscale. Therefore, the dynamic signatures associated with such modifications demand in-depth characterization. Kim *et al.*[47] have investigated segmental and chain dynamics of self-suspended nanoparticle-tethered polyisoprene suspensions. They show that, depending on grafting density, unentangled polyisoprene chains tethered to silica nanoparticles relax more slowly than their tethered, entangled counterparts. These studies bring into focus the important role of chain confinement on relaxation behaviors.

Recognizing the importance of interactions across the internal interfaces within polymer nanocomposites, in the current work, we probe the molecular and interfacial dynamics in two sets of poly(methyl methacrylate) (PMMA) nanocomposites: one set comprises bare silica nanoparticles in PMMA matrices and the other is a polymer-grafted nanocomposite consisting of PMMA-grafted silica nanoparticles (PMMA-g-NPs) in two different PMMA matrices. For brevity, we shall refer to polymer nanocomposites having bare nanoparticles simply as PNCs (polymer

nanocomposites), and those having polymer-grafted nanoparticles as PGNCs (polymer-grafted nanocomposites). Detailed analyses of the dielectric spectra reveal that while indeed one observes slower dynamic modes attributed to the interfacial layer in both PNCs and PGNCs, the distribution of relaxation times provides significant evidence for the existence of additional faster modes – in comparison to bulk PMMA – that depend on the molecular weight of the matrix and NP loading. To the best of our knowledge, this represents the first report of this phenomenon, perhaps because previous experimental efforts have not focused on the distribution of relaxation times when analyzing relaxation data for these types of systems. A challenge that is particular to analyzing the dielectric response of PMMA-based nanocomposites – which are widely studied because of their industrial relevance – is the pronounced secondary process (the beta-relaxation), which masks the primary structural relaxation, making it challenging to analyze the spectral shape of the segmental relaxation. Because of this and because faster relaxation modes are an unexpected result, we focus on changes due to the nanoparticle loading level and molecular weight of the matrix PMMA, without varying the chemistry of the PNC and PGNC surface. By detailed studies of the shape of the segmental relaxation, we argue that changes in chain packing density and chain wetting in the interfacial regions of the nanocomposite can account for the observed systematic alterations in the shape of the relaxation. From this, we offer a consistent, unifying view describing how interactions and nanoscale organization at matrix/nanoparticle and matrix/graft chain interfaces give rise to both faster and slower modes in these systems.

Experimental Methods

Synthesis of Materials

Materials and Reagents. Methyl methacrylate (MMA, 99%, Aldrich) was passed through basic alumina to remove the inhibitor. Azobisisobutyronitrile (AIBN, 98%, Aldrich) was recrystallized from methanol and dried *in vacuo* overnight. Poly(methyl methacrylate) with reported average molecular weights of 15 kg/mol and 120 kg/mol (Aldrich), 4-cyano-4-(phenylcarbonothioylthio)pentanoic acid (Aldrich), anhydrous benzene (99.8%, Aldrich), anhydrous tetrahydrofuran (THF, 99.9%, Fisher), hexanes (95%, Fisher), and (3-aminopropyl)dimethylethoxy silane (Gelest) were used as received. Unfunctionalized silica nanoparticles (Si NPs) (14 nm ± 4 nm, received as a gift from Nissan Chemical Inc.) were isolated, collected, and dried prior to use as described in our recent work.[48] These Si NPs are referred to as "bare" Si NPs.

Synthesis of Amine-Functionalized Silica Nanoparticles. Silica nanoparticles were functionalized with (3-aminopropyl)dimethylethoxy silane as described by Natarajan *et al.*[49] To accomplish this, 16 mL of Si NPs dispersed in MEK were added to a 100 mL round bottom flask containing 50 mL of THF and 0.5 mL (3-aminopropyl)dimethylethoxy silane. Next, the mixture was heated to reflux at 75 ºC for 24 h. The reaction was then quenched by precipitating the amine-functionalized nanoparticles into 400 mL of hexanes. The suspended amine-functionalized nanoparticles were transferred to a centrifuge vial and centrifuged for 10 minutes at 4000 rpm. After decanting the supernatant, the amine-modified NPs amassed at the bottom of the tube were re-dispersed by adding THF (~20 mL). To ensure unattached silanes were removed, this cycle of precipitation-

centrifugation-(re-)dispersion was completed at least three times.[49, 50] After purification, the amino-modified nanoparticles were collected and dispersed in THF until further use.

End-Functionalized PMMA Chains via RAFT Polymerization. Following protocols described by Li *et al*., a modified chain transfer agent (CTA) containing a mercaptothiazoline end group was used to create end-functionalized PMMA chains.[51] Information related to the synthesis and characterization of this modified CTA, designated as MCPBD, is relegated to the *Supporting Information.* PMMA graft chains containing a terminal mercaptothiazoline end group were polymerized by adding 9.0 g (89.9 mmol) of MMA into a 50 mL round bottom flask containing 66.1 mg (174.0 mmol) of MCPDB, 5.4 mg (32.9 mmol) of AIBN, and 20 mL of benzene. After the reagents were added, the mixture was sparged with argon for 10 minutes to remove oxygen. Next, the flask containing the reaction mixture was placed in an oil bath pre-heated to 65 °C for 18 h. Then, the polymerization was quenched by immersing the flask in liquid nitrogen. After thawing, the crude product mixture was precipitated into chilled hexanes. The precipitated polymer was collected, dissolved in THF, and then re-precipitated into hexanes again to remove residual monomer or reagents. Finally, the polymer was collected via filtration and dried *in vacuo* overnight at 40 °C. After drying, PMMA was characterized *via* gel permeation chromatography (GPC). As seen in **Figure S1**, the molecular weight of PMMA chains was determined to be 26,760 g/mol with a dispersity, Đ, of 1.09.

Synthesis of PMMA-grafted Nanoparticles. As demonstrated by Li *et al.*, the mercaptothiazoline end group is an excellent leaving group that facilitates linking with primary amines, rather than aminolysis of thioesters.[51] In addition, MCPDB is well-suited for controlled polymerization of methacrylates. For this reason, MCPDB was used to graft PMMA chains to amine-functionalized nanoparticle surfaces, resulting in PMMA-grafted nanoparticles. The experimental protocol

involved placing 0.3 g of amine-functionalized Si NPs in a 50 mL round bottom flask containing 0.52 g (0.019 mmol) of mercaptothiazoline terminated PMMA (30 kg/mol) and 20 mL of THF. The flask containing this reaction mixture was placed in an oil bath preheated to 75 °C and refluxed for 48 h. After that time, the reaction mixture was precipitated in 400 mL of chilled hexanes and the suspended polymer/polymer-grafted nanoparticle mixture was collected by centrifugation at 4000 rpm for 10 minutes. As described by Jiao and Akcora, PMMA-grafted nanoparticles (PMMA-g-NPs) can be separated from unattached (free) polymer chains by utilizing a mixed solvent precipitation procedure with THF and hexanes.[52] To accomplish this, the mixture of PMMA-g-NPs and unattached PMMA chains obtained after centrifugation were first dissolved in THF and then the non-solvent, hexanes, was added drop-wise until the solution first showed turbidity. Next, the solution was centrifuged for 10 minutes at 4000 rpm, which yields a clear supernatant layer. As described by Jiao and Akcora,[52] this layer, which contains the free polymer chains, was decanted into hexanes. The pellet of solids containing PMMA-g-NPs remaining after centrifugation were re-dissolved in THF, and this cycle was completed three times or until no polymer precipitated when the supernatant layer was decanted in hexanes. Thermal gravimetric analysis (TGA) was used to verify complete removal of PMMA-g-NPs, as seen in **Figure S2**. Finally, the PMMA-g-NPs were collected and dried overnight *in vacuo* at 50 °C to remove residual solvents. The mass loss measured by TGA via a TA Instruments Discovery Series Thermogravimetric Analyzer was used to assess the number of PMMA chains attached to the surface of Si NPs, as exemplified in **Figure S3**. A typical experimental protocol consists of placing 0.5-2 mg of PMMA-g-NPs in a 100 μL platinum high temperature pan and subjecting the sample to a temperature ramp from 30 to 800 °C at a rate of 10 °C/min. The method of calculating the grafting density of the PMMA-g-NPs, which also requires chain molecular weight measured by

GPC, is described in the following section. These analyses indicate that the grafting density of PMMA chains on the PMMA-g-NPs is 0.03 chains/nm^2.

Generation of Polymer Nanocomposites. The preparation of nanocomposites followed a procedure described by Martin *et al.* in which a blend of the inorganic additive, either bare Si NPs or PMMA-g-NPs, and a PMMA matrix was prepared by co-dissolving the PMMA-g-NPs and PMMA in THF and mixing at room temperature for 24 h.[53] The protocol for generating PMMA nanocomposites containing PMMA-g-NPs at 5 wt% (by mass, based on mass of silica only) is described as an example. TGA analysis showed that the PMMA-g-NPs had a weight loss of 25.60%, so to create a nanocomposite that is 5 wt% based on mass of silica, 6.73 mg of PMMA-g-NPs were used. Those PMMA-g-NPs were dissolved in 15 mL of THF while a separate solution consisting of 93.27 mg of the PMMA matrix (either 15 kg/mol or 120 kg/mol) in 15 mL of THF was also prepared. These solutions were sonicated for 30 minutes and then stirred for 12 h. Then, the two solutions were combined, sonicated for an additional 30 minutes and stirred overnight. The PMMA nanocomposite solution was poured into PTFE dishes and the solvent was allowed to evaporate overnight in the fume hood. Next, nanocomposites were annealed *in vacuo* at 120 °C for 24 h. All nanocomposites formulated using this procedure were characterized *via* TGA to confirm the loading level (wt% of silica) of PMMA-g-NPs before being subjected to other characterizations. The nanocomposites prepared for this study had 0, 1, 3 and 5 wt% of silica (based on mass) in PMMA matrices of either 15 or 120 kg/mol.

Characterization of Materials

A Varian VNMRS 500 MHz was used to collect ^{1}H NMR spectra at 25 °C using deuterated chloroform as the solvent (see **Figure S4**). GPC measurements were performed using an Agilent

1260 Infinity II system equipped with a Wyatt Dawn® Helios® 8 Multi-Angle Light Scattering Detector, ViscoStar® III, and an Optilab® T-rEX™. GPC measurements were conducted at 25 °C in THF with a 1 mL/min flow rate as the mobile phase. The dispersity, Đ, and number-average molecular weight, M_n, of PMMA graft chains and PMMA matrices were determined using conventional calibration analysis using polystyrene standards. A TA Instruments Q-2000 Differential Scanning Calorimeter was used to determine the glass transition temperatures (T_g) of the polymer nanocomposites. The procedure involved placing ~5 mg of the polymer nanocomposite in an aluminum pan that was subsequently subjected to a heat/cool/heat cycle from 50-160 °C at a rate of 10 °C/min using nitrogen as the purge gas. The T_g of polymer nanocomposites is reported as the temperature corresponding to the maximum of the derivative of specific heat capacity in the second heating curve. A TA Discovery Series Thermogravimetric Analyzer was used to determine the amount of silane and PMMA graft chains attached to the nanoparticle surface after each surface modification step described above. The average grafting density of PMMA chains on the nanoparticle surface, σ, was calculated using Equation 1:

$$\sigma = \left(\frac{W_{PMMA}}{100-W_{PMMA}} - \frac{W_{AMINE}}{100-W_{AMINE}}\right)\frac{N_A}{(M_n)(S_{NP})} \quad (1)$$

where N_A is Avogadro's number, M_n is the molecular weight of the PMMA grafted chains, S_{NP} is the specific surface area of the 14 nm Si NPs (calculated to be 2.07×10^{20} nm^2/g), and W_{PMMA} and W_{AMINE} represent the (percent) mass loss of PMMA-grafted NPs and the mass loss of the amine-functionalized nanoparticles, respectively, which are obtained *via* TGA. The physical characteristics of the end-functional and matrix PMMA as well as the PMMA-g-NPs are summarized in **Table S1**.

Broadband dielectric spectroscopy (BDS) experiments were performed on a Novocontrol High Resolution Alpha Analyzer equipped with a Quatro system with the capability to control temperature within 0.1 K of the set point. The polymer and polymer-nanocomposite samples were thermo-mechanically pressed into 100 μm thick films using a hot press platform at 400 K in nitrogen ambience. The films were then sandwiched between polished brass electrodes with a diameter of 15 mm to form a parallel-plate capacitor configuration. The sample thickness was ensured using 100 μm thick silica spacers. Before substantive dielectric measurements, the films were annealed at 430 K under dry nitrogen flow for ~10 hours in order to remove any adsorbed water as well as to equilibrate them. During this annealing process, the real part, ε', of the complex dielectric function at selected frequencies were monitored as a function of time. ε' increases to a maximum value as the set temperature point is reached, and eventually decays to a plateau value after several hours of annealing. Dielectric measurements were carried out in the frequency range 1 mHz to 10 MHz over cooling and heating cycles between 290 and 430 K.

Results and Discussion

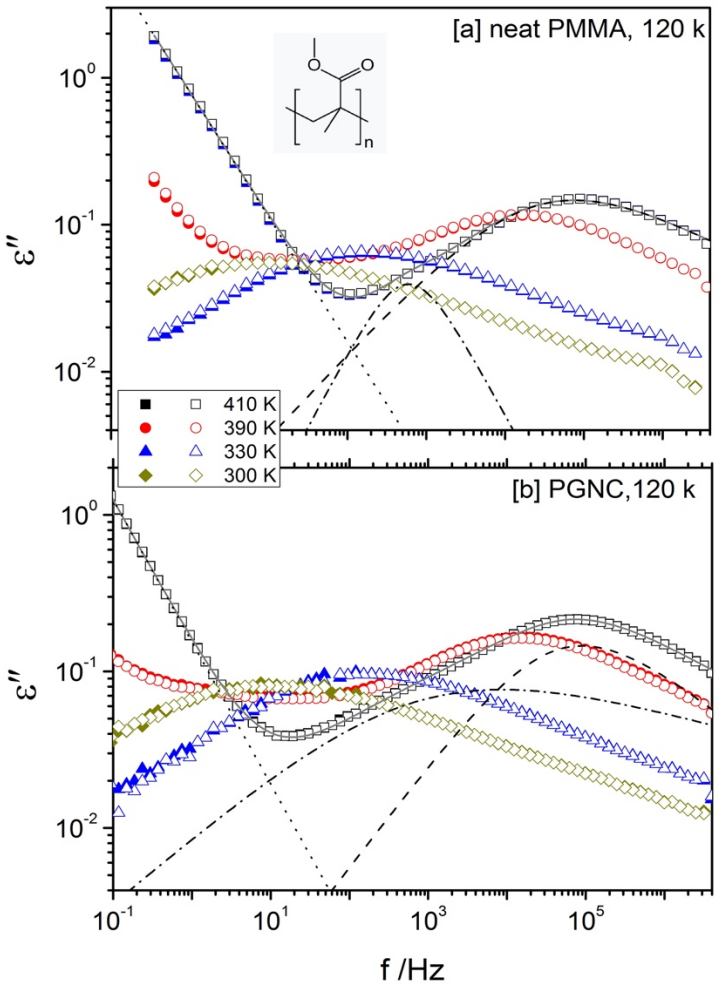

FIGURE 1: Imaginary part of the complex dielectric function, $\varepsilon^* = \varepsilon' - i\varepsilon''$, plotted as a function of frequency for (a) neat PMMA with molecular weight 120 kg/mol, and (b) PMMA-grafted silica nanoparticles (5 wt%) dispersed in PMMA matrix of 120 kg/mol. Solid symbols: spectra obtained on cooling; Open symbols: heating. The inset shows the chemical structure of PMMA. The dashed-dotted and dashed lines show HN fits to the α- and β-processes respectively, while the dotted line is the conductivity contribution at 410 K. Solid lines are the total fit functions. Details about data fitting are explained later in text. The error bars are comparable to the size of the symbols unless otherwise specified.

Figure 1 shows the imaginary part of the complex dielectric function, ε'', as measured over cooling and heating runs for the polymer matrix (neat PMMA, 120 kg/mol) and PGNC, 120 kg/mol. The coincidence between the values of the dielectric loss measured during cooling and heating runs indicates that the samples are thermally stable in the temperature range of interest. The dielectric loss spectra of PMMA exhibit a strong upturn at low-frequency due to dc ionic conductivity. The two dielectric relaxations indicated in Figure 1 are consistent with a primary

structural (α-) relaxation attributed to segmental dynamics and a β-relaxation that is due to local dipolar fluctuations of the -$COOCH_3$ groups. The latter process dominates the dielectric spectra because of the strong electric dipole associated with the carboxylate ester group. (The structure of PMMA is inset in Figure 1A.) In contrast, only a small fraction of the total electric dipole contributes to segmental dynamics reflected in the α-relaxation.[54, 55] **Figure 2** presents the dielectric relaxation spectra – for systems with a molecular weight of 120 kg/mol – recast using the derivative representation, $\varepsilon''_{der}(\omega) = (-\pi/2)[\partial\varepsilon'(\omega)/\partial ln\omega]$ (where $\varepsilon'(\omega)$ is the real part of the complex dielectric function and ω is the radial frequency of the applied electric field).[56] This representation makes the α-process easier to visualize: It shows as a shoulder on the low-frequency side of the β-process, as seen in the derivative representation of **Figure 2**. **Figure 2** also reveals subtle changes in the spectra as the system is changed from neat PMMA to PNCs to PGNCs; these changes are the subject of further analysis and discussion. To analyze the data, a combination of two empirical Havriliak-Negami (HN)[57] functions and a term accounting for dc ionic conductivity contribution is used:

$$\varepsilon^* = \mathcal{E}_\infty + \left\{\frac{\Delta\varepsilon}{\left[1+(i\omega\tau_{HN})^{\beta}\right]^{\gamma}}\right\}_{alpha} + \left\{\frac{\Delta\varepsilon}{\left[1+(i\omega\tau_{HN})^{\beta}\right]^{\gamma}}\right\}_{beta} - i\frac{\sigma_0}{\varepsilon_0\omega^s} \quad (2)$$

where $\varepsilon^* = \varepsilon' - i\varepsilon''$ is the complex dielectric function, σ_0 is the dc ionic conductivity of the sample, which presumably arises from trace impurities, ε_0 is the dielectric permittivity of vacuum, ε_∞ is the permittivity of the unrelaxed system, $\Delta\varepsilon$ is the dielectric relaxation strength, τ_{HN} is the characteristic relaxation time, and β and γ are the symmetric and asymmetric shape parameters, respectively. In addition, $\omega = 1/2\pi f$ is the angular frequency of the applied external field, and $0 \leq s \leq 1$ is a scaling parameter. The subscripts *alpha* and *beta* refer to the two relaxation processes. We use a derivative approach to extract , τ_{HN}, from the dielectric loss spectra for a

significant reason: It is a well-established fact that $\varepsilon''_{der}(\omega)$ alters the shape of the relaxation peaks but not the frequency corresponding to the peak (see Figure S5 for illustration);[58] therefore the derivative approach is used exclusively for the determination of the characteristic relaxation times, τ_{HN}, of the two relaxations. These characteristic times are then used as fixed parameters when fitting $\varepsilon''(f)$ data, which reduces the number of free parameters. Furthermore, given the fact that the β-process is a very localized relaxation, in order to uniquely determine the shape of the α-process, we invoke the assumption that at any given temperature, the peak due to the β-process is unaltered in its shape between neat PMMA and the nanocomposites. However, we do not impose this requirement on its characteristic relaxation rate. Concerning the aforesaid assumption, it is worth recalling here that the β-relaxation in methacrylate polymers is attributed to the rotation of the –COOR group about its bond with the backbone chain. In their study of several methacrylate polymers, Ribelles and Calleja[59] found that the position, shape and activation energy of the β-relaxation remains unchanged across the systems. Studies of PMMA in confinement have shown that the mean relaxation rates attributed to the β-process remain unaltered.[60-62] To the best of our knowledge, no previous studies have substantively focused on the spectral shapes of the β-relaxation for confined polymers.

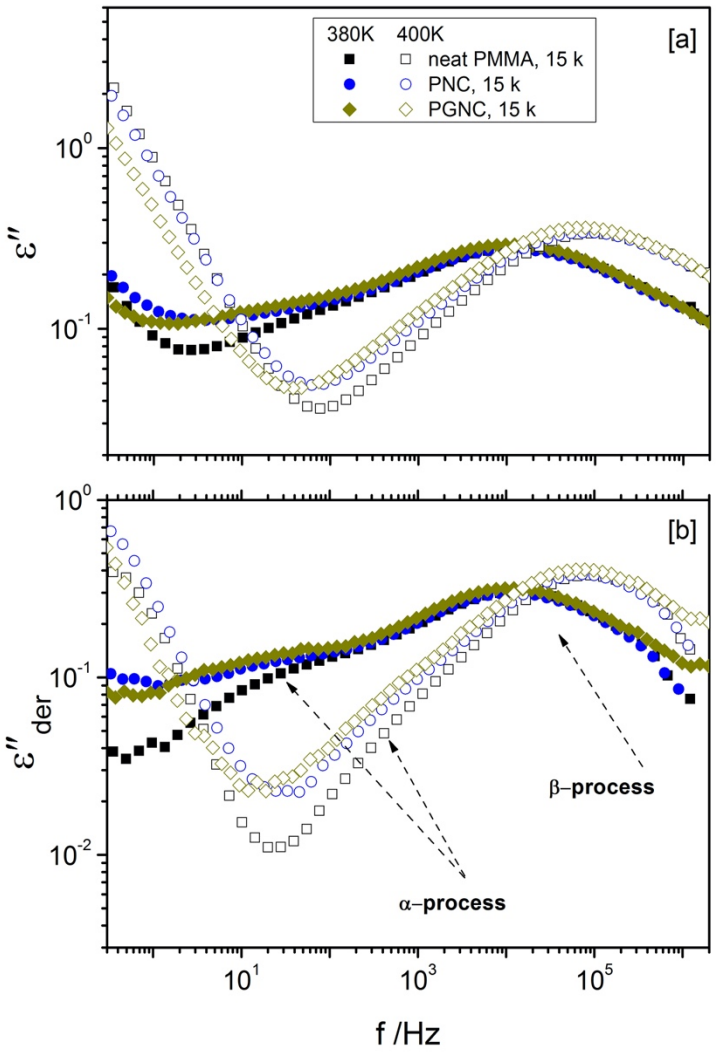

FIGURE 2: (a) Dielectric loss, ε'', versus frequency as measured at 380 and 400 K for three systems: (i) neat PMMA, 15 kg/mol; (ii) a PNC comprising 14 nm bare silica nanoparticles (NPs) dispersed in 15 kg/mol PMMA at 5 wt.% loading; and (iii) a PGNC with 5 wt% loading of PMMA-g-NPs in 15 kg/mol PMMA matrix. (b) The derivative representation of the same data calculated as $\varepsilon''_{der}(\omega) = (-\pi/2)[\partial\varepsilon'(\omega)/\partial ln\omega]$, which clearly reveals the two relaxations present in the spectra. The error bars are smaller than or comparable to the size of the symbols unless otherwise specified.

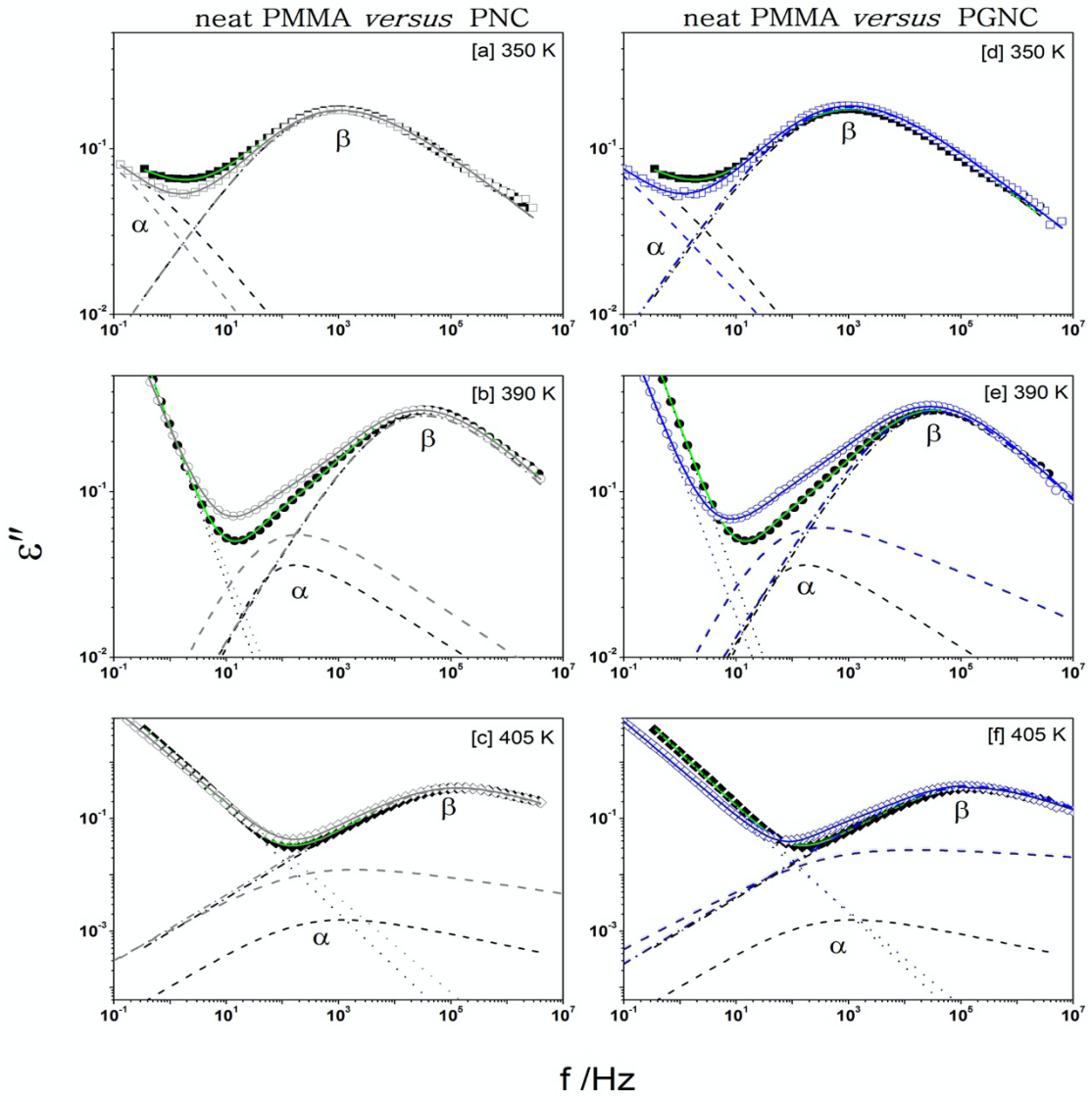

FIGURE 3: Dielectric loss, ε'', versus frequency at three selected temperatures, as indicated, for neat PMMA, 15 kg/mol (closed black symbols) compared to PNC, 15 kg/mol (open gray symbols – [a], [b] and [c]) and PGNC, 15 kg/mol (open blue symbols – [d], [e] and [f]). Depending on the temperature, and hence the relaxations observable in the accessible frequency window, data are described using either one or two Havriliak-Negami functions plus a dc ionic conductivity contribution (Eq. 2) as shown using dash-dotted lines (β-process), dashed lines (α-process) and dotted lines (conductivity contribution). The solid lines are convolutions of individual functions used to model the entire spectrum. The colors of the symbols and lines between measured data and the fit functions are kept consistent except for the black solid symbols, where – for graphical clarity – solid green lines are applied. PNCs and PGNCs are constituted at 5 wt% based on the mass of silica. The error bars are smaller than or comparable to the size of the symbols unless otherwise specified.

Figure 3 provides an illustration of the HN fit functions that are used to describe the individual relaxations as well as the complete function that captures all of the processes at three representative temperatures (350 K, 390 K, and 405 K) for systems made using the 15 kg/mol matrix PMMA. (Also see **Figure S6** in the *Supporting Information* for analogous representation of the dielectric spectra and corresponding fits for the 120 kg/mol systems.) As demonstrated by the coincidence of the solid lines and the measured data, this fitting procedure provides an excellent quantitative description of the measured spectra. The mean molecular relaxation times, τ_m, were then calculated from the HN parameters using the equation[63]

$$\tau_m = \tau_{HN} sin\left(\frac{\beta\gamma\pi}{2+2\gamma}\right)^{1/\beta} sin\left(\frac{\beta\pi}{2+2\gamma}\right)^{-1/\beta} \quad (3)$$

In **Figure 4**, these mean molecular times for the two relaxation processes are plotted as a function of inverse temperature. The solid symbols are data for the α-relaxation, while the empty ones represent the β-process. There are a variety of salient points that emerge from this figure. First, we observe that the mean relaxation rates of the β-process for neat PMMA are similar – within the limits of experimental uncertainty – to those of the polymer nanocomposites. This behavior is consistent with the understanding that the β-relaxation is a localized dipolar relaxation and therefore is hardly affected by polymer-nanofiller interactions. Boucher *et al*. made a similar observation in their study of physical aging in PMMA/silica nanocomposites.[61, 62] Second, by using an Arrhenius function, $\nu(T) = \nu_\infty \exp(-E_A/k_B T)$ (where ν_∞ is the relaxation rate in the high temperature limit, k_B the Boltzmann constant and E_A the activation energy), to describe the

β-process, we find that the activation energy of the β-relaxation changes from ~86 kJ/mol at higher temperatures to ~74 kJ/mol at lower temperatures. As illustrated in **Figure 4**, these changes occur at 384 ± 2 K and 367 ± 2 K for the 120 kg/mol and 15 kg/mol systems, respectively, which are approximately equal to the calorimetric glass transition temperature of each system, respectively. This phenomenon has been observed before in several methacrylate polymers[55, 59, 64-67] and has been assigned by some researchers to an actual change in the mechanism of the relaxation, specifically to the onset of cooperativity of the structural α-relaxation.[66, 67] However, the impact of reduction of the number of fit functions and parameters below the Tg could also lead to some shifts in the activation energies obtained. The extent to which this effect is sufficient to explain the change in the activation energy at the T_g remains unclear and is outside of the scope of the current work. Third, the α-relaxation slows as systems are progressively changed from neat PMMA to PNCs to PGNCs. This pattern corresponds to a gradual increase in T_g, which agrees with the results obtained from our DSC experiments. (See **Figure S7**.) Fitting the temperature dependence of the characteristic mean times of the α-relaxation to the Vogel-Fulcher-Tammann (VFT) equation[68-70] ($1/\tau\,(\mathrm{T}) = (1/\tau_0)\exp(-\mathrm{DT_V}/[\mathrm{T}-\mathrm{T_V}])$, where τ_0 and D are constants, and $\mathrm{T_V}$ is the Vogel temperature) and extrapolating the dependence down to 100s, we find, within experimental accuracy, a coincidence with the calorimetrically determined T_g. This coincidence is conventionally used to unambiguously identify the structural α-relaxation.[63] It should however be noted that because of the narrow temperature range in which we are able to follow the structural α-relaxation, the VFT fits applied have higher uncertainty. Nevertheless, the coincidence of the glass transition from two independent experimental methods lends credence to our assignment of the process to structural α-relaxation. Deviations from bulk T_g values for polymer nanocomposites are attributed to interfacial interactions between the polymer matrix and inorganic nanoparticles.[49,

[71] Specifically, decreases in T_g values suggest negligible or repulsive interactions across the additive/matrix interface,[8, 49, 71] while increases from bulk values are indicative of attractive particle/matrix interactions.[71-74] It is well-known that hydroxyl groups present on silica NP surfaces participate in hydrogen bonding interactions with the carbonyl groups present in each monomeric repeat unit of PMMA.[13, 74, 75] These non-bonded attractive interactions lead to slower segmental relaxation of the PMMA due to confinement of chains at the surface, which forms an interphase with reduced mobility that manifests as an increase in T_g.[48] For nanocomposites containing PMMA-grafted nanoparticles, an additional interaction is introduced: graft chains interact with the matrix polymer, which results in an increase in the number density of entanglements and interdiffusion of chains within the interfacial zone, manifesting as an increase in T_g for the polymer-grafted nanocomposites.[10, 14] Finally, the dielectric relaxation strength, $\Delta\varepsilon$, associated with the primary process increases with nanoparticle loading level and with the molecular weight of the matrix for both PNCs and PGNCs. (See Table S2.) This is due to the increased contributions due to interfacial polarization arising from the growth of the total interfacial volume in the vicinity of the particles.

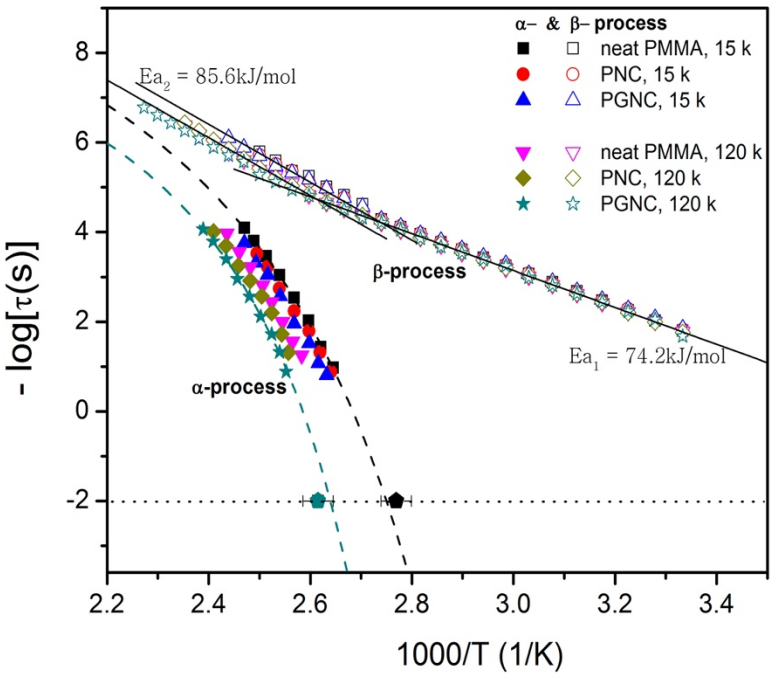

FIGURE 4: Characteristic mean relaxation times of the α- and β-process for neat PMMA and the nanocomposites studied in this work, as functions of inverse temperature, as indicated. For graphical clarity, data is shown only for neat polymers and polymer nanocomposites with 5 wt% (based on Si NPs) NP loading. The solid and dash lines are fits to the Arrhenius and VFT equations, respectively (see text for details). Representative values of T_g determined from DSC measurements for neat PMMA 15 k (black pentagon symbol) and PGNC 120 k (gray pentagon symbol) are also shown. VFT fits are displayed only for two samples for graphical clarity, and agreement between BDS and DSC data is evident. (15 k and 120 k stand for the respective molecular weight of the system in kg/mol). The error bars are smaller than or comparable to the size of the symbols unless otherwise indicated.

To gain deeper insight into the dynamics of the PNCs and PGNCs, we turn our attention to the shape of the α-peak as obtained from HN fits of the dielectric loss spectra. As noted earlier, while the mean relaxation time is appropriately characterized from the derivative spectra, the dynamic heterogeneity of the system, which is represented in the distribution of relaxation times, must be deduced from the original dielectric loss spectra. **Figure 5** shows the HN functions for the 15 kg/mol systems with different loading levels (0, 1, 3 and 5 wt% based on silica – see raw data in

Figure S8) of either bare Si NPs or PMMA-g-NPs at 390 and 405 K. An analogous plot for the 120 kg/mol systems is presented as **Figure S9** in the *Supplementary Information* document. For ease of comparison, each function is normalized with respect to the maximum dielectric loss as well as its corresponding peak frequency value. The spectral shape of the α-relaxation is observed to broaden compared to the neat PMMA, and this broadening is found to depend on temperature, molecular weight of the matrix, and NP loading level. It is instructive to note that the α-peak is accessible in a rather narrow temperature window and hence this analysis is limited to the range 390 to 405 K. At lower temperatures, PNC systems show no significant broadening in the α-relaxation process, while PGNC systems are broadened asymmetrically (specifically, skewed toward more broadening on the high-frequency side) and symmetrically for the 15 and 120 kg/mol matrices, respectively. At higher temperatures, the broadening remains skewed toward the high-frequency side for the nanocomposite made using the low molecular weight PMMA matrix, but nearly symmetrical for the PGNC made with the high molecular weight PMMA. All of these changes become more pronounced with increasing NP loading. By calculating the area under each curve, we can estimate the degree of broadening with respect to the α-peak for neat PMMA. **Table S3** presents the results from analyzing data acquired for systems made to have PMMA-g-NPs at 1 and 5 wt% loading levels. It is worth noting that throughout the article, loading levels are calculated based on Si content only.

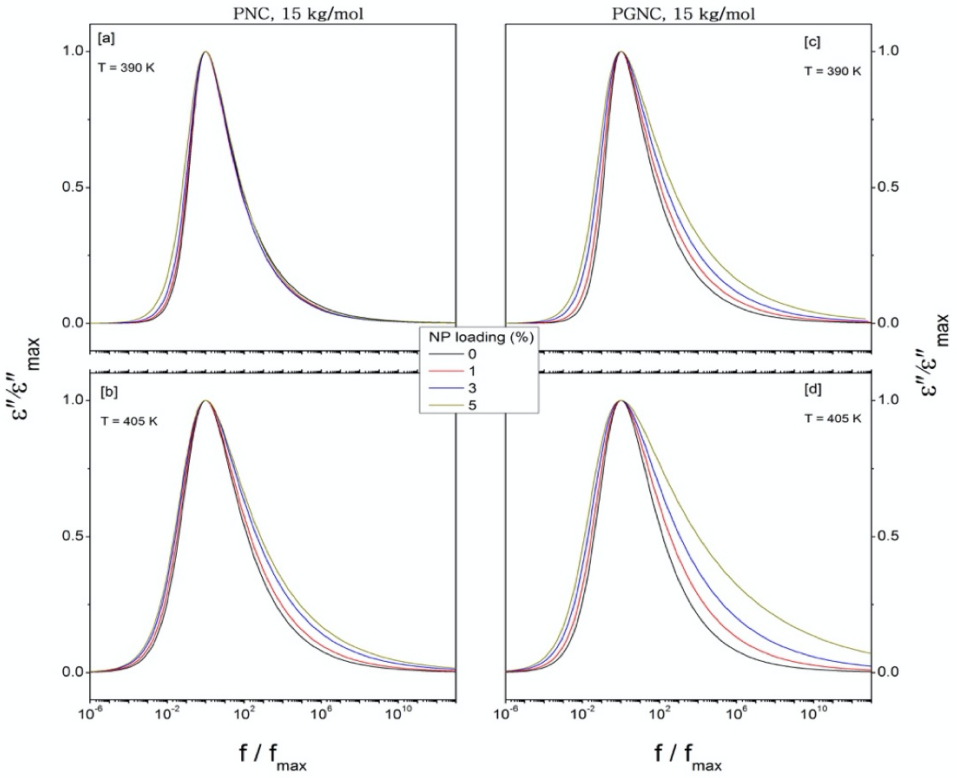

FIGURE 5: Havriliak-Negami functions that describe the α-relaxation for systems made with 15 kg/mol PMMA matrix at different loading levels of either bare NPs ([a] and [b]) or PMMA-g-NPs ([c] and [d]) at 390 and 405 K. To facilitate comparisons of the peak shapes, each function is normalized with respect to the maximum loss, ε''_{max}, as well as the corresponding peak frequency value, f_{max}. The error bars are comparable to the size of the symbols unless otherwise specified.

Broadening of the structural relaxation spectra implies a widening of the distribution of the underlying microscopic relaxation times, and hence of the dynamic heterogeneity of the system. We attribute the broadening on the low-frequency side in the current work to interfacial interactions. In the case of PNCs, there are attractive hydrogen bonding interactions between PMMA's carbonyl groups and hydroxyl groups on the surface of silica nanoparticles. These favorable polymer-NP interactions lead to the emergence of an interphase – a region wherein

dynamics are slowed – close to the nanofillers. For the case of PGNCs, polymer matrix chains, or at least some portion of the chains (for high molecular weight chains), wet and penetrate the tethered layers. This leads to confinement (i.e., reduced degrees of freedom) for those segments in the interacting region. Notably, for both PNCs and PGNCs, we do not observe a distinct new peak that could be assigned to interfacial dynamics, which has been reported for P2VP- and PVAc-based nanocomposites.[31, 32] Our findings, therefore, suggest that the interphase may be pictured, not as a layer with uniform dynamics, but rather, one with a gradient of mobilities that eventually become bulk-like as a "gedanken" molecular probe moves away from the nanoparticle. Comparison of Figures 5a and 5c with 5b and 5d shows that the fraction of modes with slower mobility is nearly temperature independent for the low-molecular weight systems (whether with bare NPs or PMMA-g-NPs), but grows with loading level for the high-molecular weight nanocomposite systems. (See **Figure S8**.) We attribute these differences to an effect of the molecular weight of the matrix, which is discussed below.

The emergence of faster relaxation modes – as seen from the broadening on the high-frequency side – is hypothesized to be a result of increased free volume. This arises from chain entanglements and interdiffusion, phenomena that should become more pronounced with increasing molecular weight of the matrix as long as the asymmetry between the graft and matrix chains is not so high that the matrix chains begin to dewet. We envision that as chains become confined in the non-uniform interphase region between hard Si NPs and the "bulk-like" matrix, packing frustrations ensue. Effectively, local non-uniform segment density leads to density fluctuations and more free volume. With this view, we posit that this effect should be more pronounced in PGNCs than PNCs because the non-uniform interphase region in the former is marked by local changes that affect the relative balance between wetting (mixing) of the graft chains by matrix chains and dewetting.[53]

Indeed and as evident from **Figures 5** and **S8**, for a given level of NP loading, the extent of broadening is greater for PGNCs than PNCs. The dependence on NP loading could be understood in the sense that increase in loading fraction – in the low loading regime studied in this work – essentially leads to higher free volume, as raising the loading level increases the amount of interphase region between NP and matrix chains per unit volume. **Figure 6** presents a schematic representation of the changes in segmental mobility that occur due to nanoparticle-matrix and matrix-graft interactions. It is emphasized that the picture emerging from the four systems probed by varying matrix molecular weight (low and high, relative to graft chain size) and type of interface (grafted and bare) is unified: the confinement of chains to the interface impedes the local segmental dynamics, but the presence of the interfacial region generated between the surface (bare or polymer-decorated) and matrix gives rise to faster modes due to an increase in free volume within the interfacial zone created by the interface between graft and matrix chains. Indeed, previous studies have demonstrated that free volume is affected by loading nanoparticles into a polymer matrix.[30, 76-78]

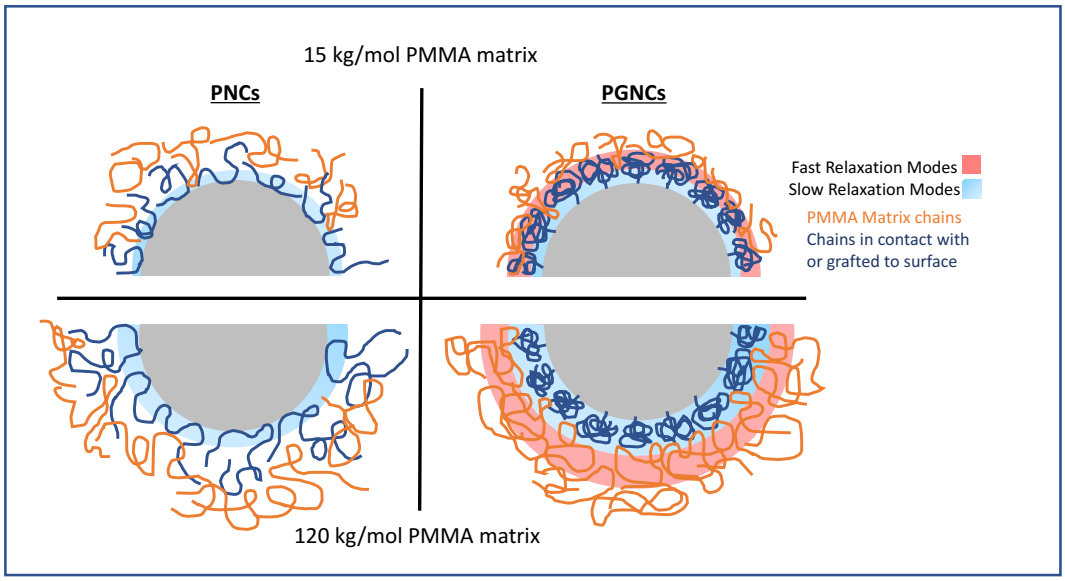

FIGURE 6: A schematic representation of polymer nanocomposites, illustrating the changes in segmental mobility that are envisioned in the vicinity of silica nanoparticles in PNCs and PGNCs.

Conclusions

We have synthesized and studied, mainly by broadband dielectric spectroscopy and differential scanning calorimetry, a series of polymer nanocomposites and polymer-grafted nanocomposites in both low- and high molecular weight matrices, specifically varying the loading levels (0, 1, 3, and 5 wt%, based on mass of the silica nanoparticles). We show that changes in the glass transition temperature depend on whether the nanoparticles are, in fact, functionalized with tethered chains. By analyzing the spectral shapes associated with the primary structural relaxation in PMMA/silica nanocomposites, the current work shows that, in terms of molecular dynamics, the main difference between PNCs and PGNCs is that the latter – depending on molecular weight of the matrix and nanofiller loading – exhibit pronounced broadening on the high-frequency side. Interestingly,

although these faster modes arise, we have found from calorimetric studies, that for a given molecular weight of the host matrix, the T_g of the PGNCs is higher than that of PNCs. This trend scales with the mean relaxation times of the α–process. We argue that faster modes for the α–relaxation are a consequence of density fluctuations as a result of chain packing frustrations due to entanglements and chain interdiffusion. The character of this non-uniform interphase region is then to be considered as an essential attribute that affects the dynamic behavior and dispersion of PNCs and PGNCs. This work provides a consistent physical picture that explains the simultaneous existence of hindered and accelerated segmental dynamics in PNCs and PGNCs, while at the same time drawing a clear difference between the two types of nanocomposite systems.

ASSOCIATED CONTENT

Supporting Information includes details of the synthesis and characterization of the modified chain transfer agent, characterizations graft chains and polymer-grafted nanoparticles, thermal properties of PGNPs, and dielectric properties of systems studied. This information is available free of charge on the ACS Publications website at pubs.acs.org.

AUTHOR INFORMATION

Corresponding Authors

*mkilbey@utk.edu, *jsangoro@utk.edu

Author Contributions

#E.U.M and D.P.S.: equal contributions

Notes

The authors declare no competing financial interest.

ACKNOWLEDGMENTS

E.U.M. and J.S. acknowledge financial support from the National Science Foundation, Division of Materials Research, Polymers Program, through DMR-1905597. S.M.K. and D.P.S. are grateful for partial support from The Department of Energy's Kansas City National Security Campus, which is operated and managed by Honeywell Federal Manufacturing & Technologies, LLC, under Contract DE-NA-0002839. In addition, S.M.K. acknowledges partial support from the National Science Foundation (CBET-1512221). Some of the dielectric measurements were performed at the UT-ORNL Joint Institute for Advanced Materials, and we thank Dr. Martin Treß and Dr. Alexei Sokolov for facilitating access to the spectrometer.

References

1. Balazs, A. C.; Emrick, T.; Russell, T. P. Nanoparticle Polymer Composites: Where Two Small Worlds Meet. *Science* **2006,** 314, 1107-1110.
2. Agrawal, A.; Choudhury, S.; Archer, L. A. A highly conductive, non-flammable polymer–nanoparticle hybrid electrolyte. *RSC Advances* **2015,** 5 (27), 20800-20809 DOI: 10.1039/c5ra01031d.
3. Wang, H.; Zeng, C.; Elkovitch, M.; Lee, L. J.; Koelling, K. W. Processing and Properties of Polymeric Nano-Composites. *Polymer Engineering and Science* **2001,** 41 (11), 2036-2046.
4. Kumar, S. K.; Benicewicz, B. C.; Vaia, R. A.; Winey, K. I. 50th Anniversary Perspective: Are Polymer Nanocomposites Practical for Applications? *Macromolecules* **2017,** 50 (3), 714-731 DOI: 10.1021/acs.macromol.6b02330.
5. Krishnamoorti, R.; Vaia, R. A. Polymer nanocomposites. *Journal of Polymer Science Part B: Polymer Physics* **2007,** 45 (24), 3252-3256 DOI: 10.1002/polb.21319.
6. Askar, S.; Li, L.; Torkelson, J. M. Polystyrene-Grafted Silica Nanoparticles: Investigating the Molecular Weight Dependence of Glass Transition and Fragility Behavior. *Macromolecules* **2017,** 50 (4), 1589-1598 DOI: 10.1021/acs.macromol.7b00079.
7. Kim, D.; Srivastava, S.; Narayananb, S.; Archer, L. A. Polymer nanocomposites: polymer and particle dynamics. *Soft Matter* **2012,** 8, 10813-10818 DOI: 10.1039/c2sm26325d.
8. Bansal, A.; Yang, H.; Li, C.; Cho, K.; Benicewicz, B. C.; Kumar, S. K.; Schadler, L. S. Quantitative equivalence between polymer nanocomposites and thin polymer films. *Nat Mater* **2005,** 4 (9), 693-8 DOI: 10.1038/nmat1447.
9. Hong, R. Y.; Fu, H. P.; Zhang, Y. J.; Liu, L.; Wang, J.; Li, H. Z.; Zheng, Y. Surface-modified silica nanoparticles for reinforcement of PMMA. *Journal of Applied Polymer Science* **2007,** 105 (4), 2176-2184 DOI: 10.1002/app.26164.
10. Rong, M. Z.; Zhang, M. Q.; Zheng, Y. X.; Zeng, H. M.; Walter, R.; Friedrich, K. Structure–property relationships of irradiation grafted nano-inorganic particle filled polypropylene composites. *Polymer* **2001,** 42, 167-183.
11. Brown, D.; Mele, P.; Marceau, S.; Alberola, N. D. A Molecular Dynamics Study of a Model Nanoparticle Embedded in a Polymer Matrix. *Macromoleclues* **2003,** 36 (4), 1395-1406 DOI: 10.1021/ma020951s.
12. Chevigny, C.; Jouault, N.; Dalmas, F.; Boué, F.; Jestin, J. Tuning the mechanical properties in model nanocomposites: Influence of the polymer-filler interfacial interactions. *Journal of Polymer Science Part B: Polymer Physics* **2011,** 49 (11), 781-791 DOI: 10.1002/polb.22246.
13. Senses, E.; Akcora, P. An Interface-Driven Stiffening Mechanism in Polymer Nanocomposites. *Macromolecules* **2013,** 46 (5), 1868-1874 DOI: 10.1021/ma302275f.
14. Bansal, A.; Yang, H.; Li, C.; Benicewicz, B. C.; Kumar, S. K.; Schadler, L. S. Controlling the thermomechanical properties of polymer nanocomposites by tailoring the polymer–particle interface. *Journal of Polymer Science Part B: Polymer Physics* **2006,** 44 (20), 2944-2950 DOI: 10.1002/polb.20926.
15. Rong, M. Z.; Zhang, M. Q.; Ruan, W. H. Surface modification of nanoscale fillers for improving properties of polymer nanocomposites: a review. *Materials Science and Technology* **2013,** 22 (7), 787-796 DOI: 10.1179/174328406x101247.
16. Ueno, K.; Inaba, A.; Kondoh, M.; Watanabe, M. Colloidal Stability of Bare and Polymer-Grafted Silica Nanoparticles in Ionic Liquids. *Langmuir* **2008,** 24 (10), 5253-5259 DOI: 10.1021/la704066v
17. Cheng, S.; Mirigian, S.; Carrillo, J. M.; Bocharova, V.; Sumpter, B. G.; Schweizer, K. S.; Sokolov, A. P. Revealing spatially heterogeneous relaxation in a model nanocomposite. *J Chem Phys* **2015,** 143 (19), 194704 DOI: 10.1063/1.4935595.

18. Gennes, P. G. d. Polymers at an interface: a simplified view. *Advances in Colloid and Interface Science* **1987,** 27, 189-209.
19. Ghanbari, A.; Rahimi, M.; Dehghany, J. Influence of Surface Grafted Polymers on the Polymer Dynamics in a Silica–Polystyrene Nanocomposite: A Coarse-Grained Molecular Dynamics Investigation. *The Journal of Physical Chemistry C* **2013,** 117 (47), 25069-25076 DOI: 10.1021/jp407109r.
20. Gin, P.; Jiang, N.; Liang, C.; Taniguchi, T.; Akgun, B.; Satija, S. K.; Endoh, M. K.; Koga, T. Revealed architectures of adsorbed polymer chains at solid-polymer melt interfaces. *Physical Review Letters* **2012,** 109 (26), 265501 DOI: 10.1103/PhysRevLett.109.265501.
21. Glomann, T.; Schneider, G. J.; Allgaier, J.; Radulescu, A.; Lohstroh, W.; Farago, B.; Richter, D. Microscopic dynamics of polyethylene glycol chains interacting with silica nanoparticles. *Physical Review Letters* **2013,** 110 (17), 178001 DOI: 10.1103/PhysRevLett.110.178001.
22. Koga, T.; Jiang, N.; Gin, P.; Endoh, M. K.; Narayanan, S.; Lurio, L. B.; Sinha, S. K. Impact of an irreversibly adsorbed layer on local viscosity of nanoconfined polymer melts. *Physical Review Letters* **2011,** 107 (22), 225901 DOI: 10.1103/PhysRevLett.107.225901.
23. Bogoslovov, R. B.; Roland, C. M.; Ellis, A. R.; Randall, A. M.; Robertson, C. G. Effect of Silica Nanoparticles on the Local Segmental Dynamics in Poly(vinyl acetate). *Macromolecules* **2008,** 41, 1289-1296 DOI: 10.1021/ma702372a
24. Carroll, B.; Cheng, S.; Sokolov, A. P. Analyzing the Interfacial Layer Properties in Polymer Nanocomposites by Broadband Dielectric Spectroscopy. *Macromolecules* **2017,** 50 (16), 6149-6163 DOI: 10.1021/acs.macromol.7b00825.
25. Jouault, N.; Jestin, J. Intra- and Interchain Correlations in Polymer Nanocomposites: A Small-Angle Neutron Scattering Extrapolation Method. *ACS Macro Letters* **2016,** 5 (10), 1095-1099 DOI: 10.1021/acsmacrolett.6b00500.
26. Cheng, S.; Holt, A. P.; Wang, H.; Fan, F.; Bocharova, V.; Martin, H.; Etampawala, T.; White, B. T.; Saito, T.; Kang, N. G.; Dadmun, M. D.; Mays, J. W.; Sokolov, A. P. Unexpected Molecular Weight Effect in Polymer Nanocomposites. *Phys Rev Lett* **2016,** 116 (3), 038302 DOI: 10.1103/PhysRevLett.116.038302.
27. Gong, S.; Chen, Q.; Moll, J. F.; Kumar, S. K.; Colby, R. H. Segmental Dynamics of Polymer Melts with Spherical Nanoparticles. *ACS Macro Letters* **2014,** 3 (8), 773-777 DOI: 10.1021/mz500252f.
28. Jouault, N.; Moll, J. F.; Meng, D.; Windsor, K.; Ramcharan, S.; Kearney, C.; Kumar, S. K. Bound Polymer Layer in Nanocomposites. *ACS Macro Letters* **2013,** 2 (5), 371-374 DOI: 10.1021/mz300646a.
29. Cheng, S.; Carroll, B.; Lu, W.; Fan, F.; Carrillo, J.-M. Y.; Martin, H.; Holt, A. P.; Kang, N.-G.; Bocharova, V.; Mays, J. W.; Sumpter, B. G.; Dadmun, M.; Sokolov, A. P. Interfacial Properties of Polymer Nanocomposites: Role of Chain Rigidity and Dynamic Heterogeneity Length Scale. *Macromolecules* **2017,** 50 (6), 2397-2406 DOI: 10.1021/acs.macromol.6b02816.
30. Harton, S. E.; Kumar, S. K.; Yang, H.; Koga, T.; Hicks, K.; Lee, H.; Mijovic, J.; Liu, M.; Vallery, R. S.; Gidley, D. W. Immobilized Polymer Layers on Spherical Nanoparticles. *Macromolecules* **2010,** 43 (7), 3415-3421 DOI: 10.1021/ma902484d.
31. Holt, A. P.; Griffin, P. J.; Bocharova, V.; Agapov, A. L.; Imel, A. E.; Dadmun, M. D.; Sangoro, J. R.; Sokolov, A. P. Dynamics at the Polymer/Nanoparticle Interface in Poly(2-vinylpyridine)/Silica Nanocomposites. *Macromolecules* **2014,** 47 (5), 1837-1843 DOI: 10.1021/ma5000317.
32. Füllbrandt, M.; Purohit, P. J.; Schönhals, A. Combined FTIR and Dielectric Investigation of Poly(vinyl acetate) Adsorbed on Silica Particles. *Macromolecules* **2013,** 46, 4626-4632 DOI: 10.1021/ma400461p.
33. Carrillo, J.-M. Y.; Cheng, S.; Kumar, R.; Goswami, M.; Sokolov, A. P.; Sumpter, B. G. Untangling the Effects of Chain Rigidity on the Structure and Dynamics of Strongly Adsorbed Polymer Melts. *Macromolecules* **2015,** 48 (12), 4207-4219 DOI: 10.1021/acs.macromol.5b00624.

34. Sargsyan, A.; Tonoyan, A.; Davtyan, S.; Schick, C. The amount of immobilized polymer in PMMA SiO2 nanocomposites determined from calorimetric data. *European Polymer Journal* **2007,** 43 (8), 3113-3127 DOI: 10.1016/j.eurpolymj.2007.05.011.
35. Holt, A. P.; Bocharova, V.; Cheng, S.; Kisliuk, A. M.; White, B. T.; Saito, T.; Uhrig, D.; Mahalik, J. P.; Kumar, R.; Imel, A. E.; Etampawala, T.; Martin, H.; Sikes, N.; Sumpter, B. G.; Dadmun, M. D.; Sokolov, A. P. Controlling Interfacial Dynamics: Covalent Bonding versus Physical Adsorption in Polymer Nanocomposites. *ACS Nano* **2016,** 10 (7), 6843-52 DOI: 10.1021/acsnano.6b02501.
36. Cheng, S.; Xie, S. J.; Carrillo, J. Y.; Carroll, B.; Martin, H.; Cao, P. F.; Dadmun, M. D.; Sumpter, B. G.; Novikov, V. N.; Schweizer, K. S.; Sokolov, A. P. Big Effect of Small Nanoparticles: A Shift in Paradigm for Polymer Nanocomposites. *ACS Nano* **2017,** 11 (1), 752-759 DOI: 10.1021/acsnano.6b07172.
37. Betancourt, B. A.; Douglas, J. F.; Starr, F. W. Fragility and cooperative motion in a glass-forming polymer-nanoparticle composite. *Soft Matter* **2013,** 9 (1), 241-254 DOI: 10.1039/C2SM26800K.
38. Kim, S. Y.; Meyer, H. W.; Saalwächter, K.; Zukoski, C. F. Polymer Dynamics in PEG-Silica Nanocomposites: Effects of Polymer Molecular Weight, Temperature and Solvent Dilution. *Macromolecules* **2012,** 45 (10), 4225-4237 DOI: 10.1021/ma300439k.
39. Zhang, Q.; Archer, L. A. Poly(ethylene oxide)/Silica Nanocomposites: Structure and Rheology. *Langmuir* **2002,** 18, 10435-10442 DOI: 10.1021/la026338j
40. Berriot, J.; Lequeux, F.; Monnerie, L.; Montes, H.; Long, D.; Sotta, P. Filler–elastomer interaction in model filled rubbers, a 1H NMR study. *Journal of Non-Crystalline Solids* **2002,** 307-310, 719-724.
41. Kaufman, S.; Splichter, W. P.; Davis, D. D. Nuclear Magnetic Resonance Study of Rubber-Carbon Black Interactions. *Journal of Polymer Science: Part A-2* **1971,** 9, 829-839.
42. Krutyeva, M.; Wischnewski, A.; Monkenbusch, M.; Willner, L.; Maiz, J.; Mijangos, C.; Arbe, A.; Colmenero, J.; Radulescu, A.; Holderer, O.; Ohl, M.; Richter, D. Effect of nanoconfinement on polymer dynamics: surface layers and interphases. *Phys Rev Lett* **2013,** 110 (10), 108303 DOI: 10.1103/PhysRevLett.110.108303.
43. Bagwe, R. P.; Hilliard, L. R.; Tan, W. Surface Modification of Silica Nanoparticles to Reduce Aggregation and Nonspecific Binding. *Langmuir* **2006,** 22 (9), 4357-4362 DOI: 10.1021/la052797j.
44. Ganesan, V.; Jayaraman, A. Theory and simulation studies of effective interactions, phase behavior and morphology in polymer nanocomposites. *Soft Matter* **2014,** 10 (1), 13-38 DOI: 10.1039/c3sm51864g.
45. Kumar, S. K.; Jouault, N.; Benicewicz, B.; Neely, T. Nanocomposites with Polymer Grafted Nanoparticles. *Macromolecules* **2013,** 46 (9), 3199-3214 DOI: 10.1021/ma4001385.
46. Pandey, Y. N.; Papakonstantopoulos, G. J.; Doxastakis, M. Polymer/Nanoparticle Interactions: Bridging the Gap. *Macromolecules* **2013,** 46 (13), 5097-5106 DOI: 10.1021/ma400444w.
47. Kim, S. A.; Mangal, R.; Archer, L. A. Relaxation Dynamics of Nanoparticle-Tethered Polymer Chains. *Macromolecules* **2015,** 48 (17), 6280-6293 DOI: 10.1021/acs.macromol.5b00791.
48. Street, D. P.; Mah, A. H.; Patterson, S.; Pickel, D. L.; Bergman, J. A.; Stein, G. E.; Messman, J. M.; Kilbey, S. M. Interfacial interactions in PMMA/silica nanocomposites enhance the performance of parts created by Fused Filament Fabrication. *Polymer* **2018,** 157, 87-94 DOI: 10.1016/j.polymer.2018.10.004.
49. Natarajan, B.; Li, Y.; Deng, H.; Brinson, L. C.; Schadler, L. S. Effect of Interfacial Energetics on Dispersion and Glass Transition Temperature in Polymer Nanocomposites. *Macromolecules* **2013,** 46 (7), 2833-2841 DOI: 10.1021/ma302281b.
50. Li, Y.; Benicewicz, B. C. Functionalization of Silica Nanoparticles via the Combination of Surface-Initiated RAFT Polymerization and Click Reactions. *Macromoleclues* **2008,** 41 (21), 7986-7992 DOI: 10.1021/ma801551z.
51. Li, C.; Han, J.; Ryu, C. Y.; Benicewicz, B. C. A Versatile Method To Prepare RAFT Agent Anchored Substrates and the Preparation of PMMA Grafted Nanoparticles. *Macromolecules* **2006,** 39 (9), 3175-3183 DOI: 10.1021/ma051983t.

52. Jiao, Y.; Akcora, P. Assembly of Polymer-Grafted Magnetic Nanoparticles in Polymer Melts. *Macromolecules* **2012,** 45 (8), 3463-3470 DOI: 10.1021/ma3000576.
53. Martin, T. B.; Mongcopa, K. I.; Ashkar, R.; Butler, P.; Krishnamoorti, R.; Jayaraman, A. Wetting-Dewetting and Dispersion-Aggregation Transitions Are Distinct for Polymer Grafted Nanoparticles in Chemically Dissimilar Polymer Matrix. *J Am Chem Soc* **2015,** 137 (33), 10624-31 DOI: 10.1021/jacs.5b05291.
54. Schmidt-Rohr, K.; Kulik, A. S.; Beckham, H. W.; Ohlemacher, A.; Pawelzik, U.; Boeffel, C.; Spiess, H. W. Molecular Nature of the Beta-Relaxation in Poly(methyl methacrylate) Investigated by Multidimensional NMR. *Macromolecules* **1994,** 27, 4733-4745 DOI: 10.1021/ma00095a014,.
55. Bergman, R.; Alvarez, F.; Alegría, A.; Colmenero, J. The merging of the dielectric α- and β-relaxations in poly-(methyl methacrylate). *The Journal of Chemical Physics* **1998,** 109 (17), 7546-7555 DOI: 10.1063/1.477376.
56. Wübbenhorst, M.; Turnhout, J. v. Analysis of complex dielectric spectra. I. One-dimensional derivative techniques and three-dimensional modelling. *Journal of Non-Crystalline Solids* **2002,** 305, 40-49.
57. Havriliak, S.; Negami, S. A Complex Plane Representation of Dielectric and Mechanical Relaxation Processes in Some Polymers. *Polymer* **1967,** 8, 161-210.
58. Heres, M.; Cosby, T.; Mapesa, E. U.; Sangoro, J. Probing Nanoscale Ion Dynamics in Ultrathin Films of Polymerized Ionic Liquids by Broadband Dielectric Spectroscopy. *ACS Macro Letters* **2016,** 5 (9), 1065-1069 DOI: 10.1021/acsmacrolett.6b00601.
59. Ribelles, J. L. G.; Calleja, R. D. The beta Dielectric Relaxation in some Methacrylate Polymers. *Journal of Polymer Science: Polymer Physics Edition* **1985,** 23, 1297-1307.
60. Serghei, A.; Mikhailova, Y.; Huth, H.; Schick, C.; Eichhorn, K. J.; Voit, B.; Kremer, F. Molecular dynamics of hyperbranched polyesters in the confinement of thin films. *Eur Phys J E Soft Matter* **2005,** 17 (2), 199-202 DOI: 10.1140/epje/i2005-10009-7.
61. Boucher, V. M.; Cangialosi, D.; Alegrìa, A.; Colmenero, J.; González-Irun, J.; Liz-Marzan, L. M. Physical aging in PMMA/silica nanocomposites: Enthalpy and dielectric relaxation. *Journal of Non-Crystalline Solids* **2011,** 357 (2), 605-609 DOI: 10.1016/j.jnoncrysol.2010.05.091.
62. Cangialosi, D.; Boucher, V. M.; Alegría, A.; Colmenero, J. Enhanced physical aging of polymer nanocomposites: The key role of the area to volume ratio. *Polymer* **2012,** 53 (6), 1362-1372 DOI: 10.1016/j.polymer.2012.01.033.
63. Kremer, F.; Schönhals, A., *Broadband Dielectric Spectroscopy*. Springer: Berlin, 2003.
64. Bergman, R.; Alvarez, F.; Alegria, A.; Colmenero, J. Dielectric relaxation in PMMA revisited. *Journal of Non-Crystalline Solids* **1998,** 235-237, 580-583.
65. Sasabe, H.; Saito, S. Dielectric Relaxations and Electrical Conductivities of Poly(alkyl Methacrylates) under High Pressure. *Journal of Polymer Science* **1968,** 6, 1401-1418.
66. Garwe, F.; Schönhals, A.; Lockwenz, H.; Beiner, M.; Schröter, K.; Donth, E. Influence of Cooperative alpha-Dynamics on Local *Macromoleclues* **1996,** 29 (1), 247-253.
67. Garwe, F.; Schönhals, A.; Beiner, M.; Schröter, K.; Donth, E. Molecular cooperativity against locality at glass transition onset in poly(n butyl methacrylate). *J. Phys.: Condes. Matter* **1994,** 6, 6941-6945.
68. Fulcher, G. S. Analysis of recent measurements of the viscosity of glasses - Reprint. *Journal of the American Chemical Society* **1992,** 75, 1043-1059.
69. Tammann, V. G.; Hesse, W. Die Abhaengigkeit der Viscositaet von der Temperatur bei unterkuehlten Fluessigkeiten. *Zeitschrift fuer anorganische und allgemeine* **1925**, 245-257.
70. Vogel, H. The law of the relationship between viscosity of liquids and the temperature. *Physikalische Zeitschrift* **1921,** 22, 645-646.
71. Ash, B. J.; Siegel, R. W.; Schadler, L. S. Mechanical Behavior of Alumina/Poly(methyl methacrylate) Nanocomposites. *Macromoleclues* **2004,** 37 (4), 1358-1369 DOI: 10.1021/ma0354400.

72. Salavagione, H. J.; Martínez, G.; Gómez, M. A. Synthesis of poly(vinyl alcohol)/reduced graphite oxide nanocomposites with improved thermal and electrical properties. *Journal of Materials Chemistry* **2009,** 19 (28), DOI: 10.1039/b904232f.
73. Ramanathan, T.; Stankovich, S.; Dikin, D. A.; Liu, H.; Shen, H.; Nguyen, S. T.; Brinson, L. C. Graphitic nanofillers in PMMA nanocomposites—An investigation of particle size and dispersion and their influence on nanocomposite properties. *Journal of Polymer Science Part B: Polymer Physics* **2007,** 45 (15), 2097-2112 DOI: 10.1002/polb.21187.
74. Rittigstein, P.; Priestley, R. D.; Broadbelt, L. J.; Torkelson, J. M. Model polymer nanocomposites provide an understanding of confinement effects in real nanocomposites. *Nat Mater* **2007,** 6 (4), 278-82 DOI: 10.1038/nmat1870.
75. Akcora, P.; Kumar, S. K.; García Sakai, V.; Li, Y.; Benicewicz, B. C.; Schadler, L. S. Segmental Dynamics in PMMA-Grafted Nanoparticle Composites. *Macromolecules* **2010,** 43 (19), 8275-8281 DOI: 10.1021/ma101240j.
76. Sharma, S. K.; Sudarshan, K.; Sahu, M.; Pujari, P. K. Investigation of free volume characteristics of the interfacial layer in poly(methyl methacrylate)–alumina nanocomposite and its role in thermal behaviour. *RSC Advances* **2016,** 6 (72), 67997-68004 DOI: 10.1039/c6ra07051e.
77. Harms, S.; Rätzke, K.; Faupel, F.; Schneider, G. J.; Willner, L.; Richter, D. Free Volume of Interphases in Model Nanocomposites Studied by Positron Annihilation Lifetime Spectroscopy. *Macromolecules* **2010,** 43 (24), 10505-10511 DOI: 10.1021/ma1022692.
78. Sharma, S. K.; Prakash, J.; Sudarshan, K.; Sen, D.; Mazumder, S.; Pujari, P. K. Structure at Interphase of Poly(vinyl alcohol)–SiC Nanofiber Composite and Its Impact on Mechanical Properties: Positron Annihilation and Small-Angle X-ray Scattering Studies. *Macromolecules* **2015,** 48 (16), 5706-5713 DOI: 10.1021/acs.macromol.5b01095.